Preparation of novel N-CNT nanocomposite as an adsorbent for removal of As+3 toxic ions and DFT calculation

Seyyed Salar Meshkat (s.meshkat@che.uut.ac.ir)
Urmia University of Technology
Zeinab Hoseini
Romina Mehrabi
Ebrahim Ghasemy
Mehdi Esrafili

Research Article

Keywords: RAFT polymerization method, N doped CNT, Heavy metal, Adsoorption

Posted Date: February 15th, 2022

DOI: https://doi.org/10.21203/rs.3.rs-1352943/v1

Preparation of novel N-CNT nanocomposite as an adsorbent for removal of As^{+3} toxic ions and DFT calculation

Seyyed Salar Meshkat[1*], Zeinab Hoseini[1], Romina Mehrabi[2], Ebrahim Ghasemy[3], Mehdi Esrafili[3]

[1]*Faculty of Chemical Engineering, Urmia University of Technology, Urmia, Iran*

[2] *Department of Materials and Metallurgical Engineering, Iran University of Science and Technology, Iran*

[3] *Institut national de la recherché, Centre Énergie Matériaux Télécommunications, 1650 Boul. Lionel-Boulet, Varennes, Quebec, J3X 1S2 Canada*

[4]*Department of Chemistry, Faculty of Basis Sciences, University of Maragheh, P.O. Box 55136-553, Maragheh, Iran*

*Corresponding authors: s.meshkat@che.uut.ac.ir

Abstract

This work aimed at developing novel adsorbents to remove arsenic ions in an aqueous solution. To this end, the use of polymeric materials and functionalized nitrogen-doped carbon nanotubes (N-CNT) was considered to adsorb arsenic ions from aqueous solutions. In this regard, the effects of experimental parameters including pH, contact time, initial concentration of metal, and the adsorption temperature were studied. According to experiments, the optimum solution pH for arsenic adsorption at 20 °C was 7. As the contact time increased, the adsorption rate increased and reached equilibrium after 10 minutes. The arsenic adsorption capacity of Polyether Sulfone/N-CNT nanocomposites increased with increasing temperature. The highest adsorption capacity was achieved at 49 °C. The equilibrium data obtained in the initial concentration range of Arsenic and the studied temperature was consistent with the Freundlich isotherm. The adsorption kinetics revealed that the arsenic adsorption followed the Pseudo-First order and Weber Morris equation. The thermodynamic parameters (ΔH, ΔG, and ΔS) indicated that the arsenic adsorption in the temperature range of 332-296 K was spontaneous and endothermic. The adsorption properties of the modified N-doped carbon nanotubes towards arsenic ions were also studied by density functional theory (DFT) calculations.

Keywords: RAFT polymerization method, N doped CNT, Heavy metal, Adsoorption.

1. Introduction

Many efforts have been devoted to synthesizing polymer nanoparticles in recent years, considering their less weight and more corrosion resistance than metal nanoparticles. Among the polymer nanoparticles, the main focus has been on the particles with specific structure and morphology, due to their various applications in impact improvement, biomedical, drug delivery, optics, and their electrical and magnetic properties [1-5]. In general, there are two synthetic and non-synthetic methods for the synthesis of these particles; non-synthetic methods can be employed to prepare aerosols and drops in very dilute polymer solutions or gas atomization of polymer melts or stretching and self-arrangement. One of the most important features of non-synthetic methods is the production of particles with a uniform size distribution [6]. Direct synthesis of these particles is possible by heterogeneous polymerization, which includes emulsion, suspension, and dispersion polymerization. In recent years, the above three methods of dispersion polymerization and granular dispersion have been used more frequently due to the ease of controlling various reaction parameters and the production of monodisperse particles. There are several methods for polymerization of chain growths: free radical polymerization, ionic, group transfer, and coordinative polymerization. Free radical polymerization is used more than others. Ion polymerization and group transfer are not widely used in industry [7]. However, they can produce better pre-designed polymers than radical polymerization. In conventional living polymerization, a suitable initiator decomposes into starting ions in a very short time and with full efficiency, and by forming active ionic centers, the starting reaction occurs. Depending on the solvent, polymerization may occur by pairing the solvent-coated ions with free ions after forming the maximum number of chain centers. One of the limitations of free radical polymerization is the lack of control over the structure of the polymer, which is due to the slow start, rapid diffusion, and

inherent end-chain reactions. Indeed, the release of newly produced radicals and their termination is done in the same second. Such a short service life prevents any tampering or control over the structure of the polymer chains produced. The advent of so-called controlled polymerization (CLRP) methods provided a new impetus for the synthesis of predetermined macromolecules using free radical polymerization [8-9]. These methods combine the inherent advantages of conventional free radical polymerization with living polymerization methods. Compared to classical free radical processes, these methods can synthesize functional homopolymers and block copolymers with predetermined molecular mass, low poly dispersion, and predictable end groups that are very difficult to obtain. These new CLRP methods are more tolerant than functional groups on monomers of classical living polymerization methods and can be performed in conventional solvents over a wide range of temperatures. They also provide easy access to the architectural design of complex polymers [9-11]. It is concluded from literature review that, the polymeric adsorbents have mostly low capacity and low efficiency in heavy metal ions adsorption. But, modified N-CNTs have been widely used as excellent materials for the removal of various heavy metals from aqueous solutions with hgh adsorption capacity and efficiency [12-14].

Inorder to modify the surface properties of the adsorbent, the surface functionalization of CNT is a highly efficient method. By this method the improper aggregation characteristics of the synthesized adsorbent can be controled. This surface control make the CNTs as a reliable and reachable adsorbent for scientists and industries to design and synthesize new nanocomposites to service CNTs in the various important technical fields. It is important to develope an actual and economical adsorbent to eliminate heavy metals from wastewaters. The adsorbent functional groups content plays an important role in reaching an effective and selective heavy metal ions adsorbents to eliminate from wastewater [15-16].

In this study, living/controlled radical polymerization was used to modify the carbon nanotube surface, due to the limitations of conventional radical polymerization. So, various living radical polymerization methods that can be used to modify the surface were discussed. Furthermore, the adsorption properties of As^{3+} ions over the modified nitrogen-doped CNTs were thoroughly studied using density functional theory (DFT) calculations. However, the novelty of this study was observed in the use of N-CNT substrate with unique properties as well as RAFT polymerization method with special advantages.

2. Experimental

2.1. Materials and methods

Various materials such as acrylic acid (AA, Aldrich), acrylamide (AAm, Aldrich), MWCNTs (OD: 5-15mm), -2,2 tetrabutylammonium hydrogen sulfate (Merck), Sulfuric acid (Merck), N and N '-carbide Imodium cyclohexene (Sigma-Aldrich), N, N' - dimethylformamide (DMF, Aldrich), 4-dimethylaminopyridine (DMAP, Aldrich), carbon disulfide and chloroform (Merck) were used in this study. In addition, recrystallization of methanol was done by azobisisobutyronitrile (AIBN, Aldrich). At end, a solution of arsenic ions (1.00 g per 10 mL of HNO_3 solution) was set.

2.1.1. RAFT factor synthesis

The BDACT was used as the chain transfer factor (CTA) and synthesized as follows [17]; Carbon disulfide (10.87m K, 0.18mol), chloroform (36.25mL), acetone (L33m), and tetrabutylammonium hydrogen sulfate (gr1) with 60mL toluene in 500ml under nitrogen gas medium have been joint. In addition, sodium hydroxide (100.8g) was mixed and stirred for 24 hours. In the next step, under the nitrogen atmosphere, 300 mL distilled water was added to the mixture to produce a two-phase layer and precipitated by 50 ml of 6.42 g of RAFT hydrochloric acid and after filtration.

2.1.2. Synthesis of N-CNT-RAFT agent

The N-CNT was synthesized as reported in our previous work [17]. The connecting factor on the N-CNT surface was created according to the following method: First, N-CNT-OH (0.5g) was added to DMF solution (40 mL) and ultrasonically dispersed for 15 minutes, then RA (BDATC, 1g) was added to the reaction medium. Certain amounts of DCC (6 g) and DMAP (0.45 g) were added to the mixture and stirred at 25 °C for 24 h. The precipitates were then washed with THF solution and dried in a vacuum oven at 40 °C. Figure 1 shows the schematic of the N-CNT-RAFT agent.

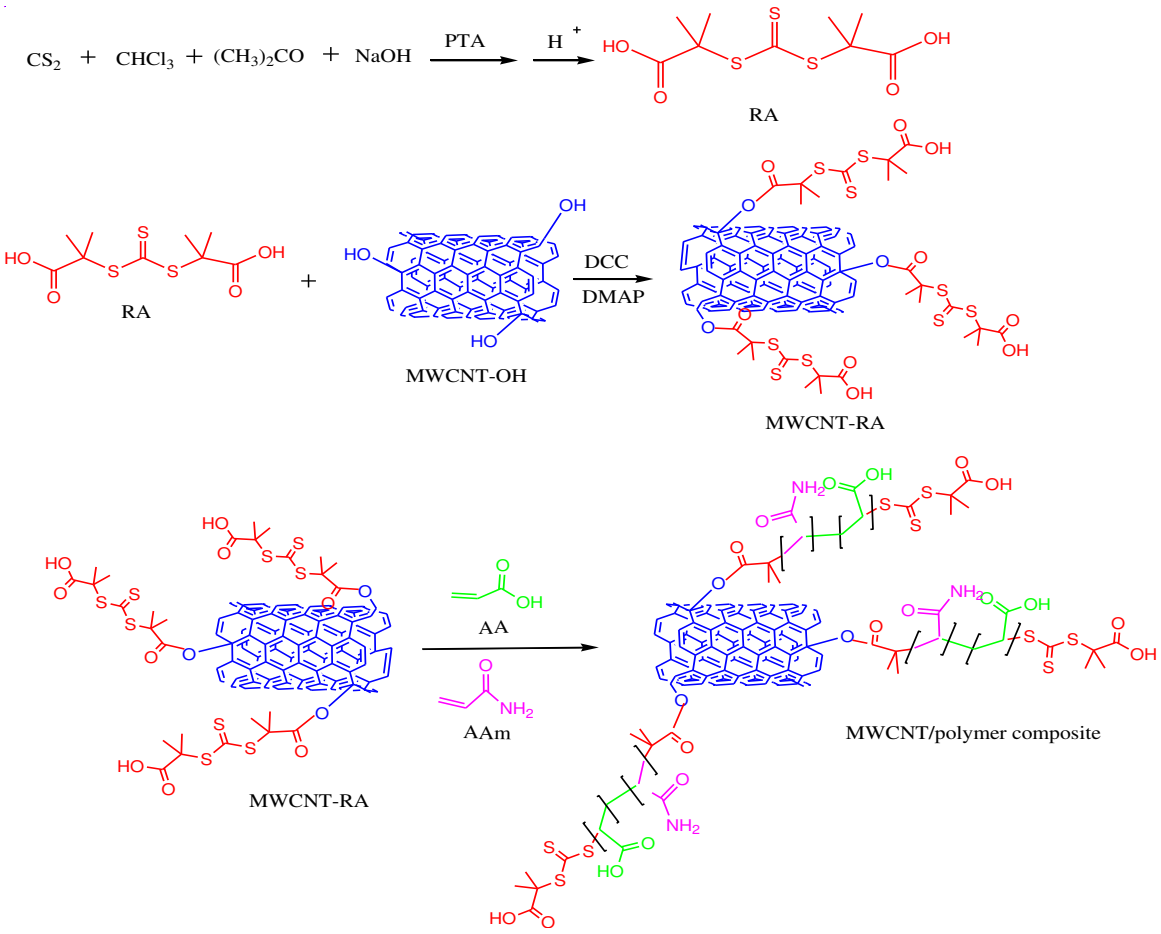

Figure 1. Scheme of the RAFT, N-CNT-RAFT agent preparation method, and N-CNT surface modification by RAFT polymerization by AAm and AA monomers

2.1.3. Synthesis of N-doped carbon nanocomposite nanotubes

The N-CNT/polymer nanocomposite was synthesized using the RAFT method and the N-CNT-RAFT precipitation agent was employed to control the copolymerization of AAm and AA monomers according to the following instructions. N-CNT-RAFT (30mg) was dispersed by ultrasonication for 20 min in 1 and 4 dioxane (10 mL), followed by the addition of AAm (0.4g), AA (0.11g), and AIBN (2.0g) monomers as initiators to the reactor. After deoxygenation, the reaction was performed at 70 ° C for 5 h. After the reaction, the contents of the reactor were transferred into cold diethyl ether (100 mL) to precipitate the nanocomposite. The final nanocomposite was obtained in gray color (0.40g, efficiency 78%).

2.2. Adsorption of Arsenic by nanocomposites

Adsorption experiments were performed using a stirrer in a batch condition. The total volume of the used solutions was 100 ml, and after each experiment, the adsorbent was separated from the solution by filtration, and the adsorbate was prepared for atomic adsorption analysis.

The optimum parameters for the arsenic adsorption process such as temperature, adsorbent mass, contact time, Arsenic initial concentration, and pH were gained from parallel batch experiments via response surface methodology (RSM) design of experiment software.

The removal efficiency for this series of experiments was obtained from Equation (1):

$$\% \text{ Removal} = \frac{(C_i - C_f)}{C_i} \times 100 \quad (1)$$

where C_i is the initial concentration and C_f is the final concentration of the adsorbed material.

q_t was also calculated from Equation (2):

$$q_t = (C_i - C_t) \times \frac{V}{m} \quad (2)$$

where C_i and C_t are the initial concentration and the concentration at time t. V is the volume of the solution, and m is the mass of the adsorbent [18].

The adsorption capacity (q_e) was calculated from Equation (3-3):

$$q_e = (C_i - C_e) \times \frac{V}{m} \quad (3)$$

Where C_i and C_e are the initial and equilibrium concentrations, and V and m were used according to the above definition [19].

2.3.Characterization

The chemical structure and morphology of synthesized nanocomposite were investigated using Philips, XL30 scanning electron microscopy (SEM) and JEOL 1200 EXII Transmission electron microscopy (TEM). X-ray diffraction (XRD) pattern of synthesized nanoparticles were obtained by PW- 1840 Philips diffractometer with Lump Cu-kα and λ = 1.54 Å using standard diffraction procedure. The molecular structure of CNT-nanocomposite was studied Fourier-transform infrared spectroscopy (FT-IR) by means of Shimadzu 8400 S. To adequately support accurate structural dereplication and specificity, the H Nuclear Magnetic Resonance (HNMR) spectra were calculated from the synthesized nanocomposite.

2.4. Computational details

To get detailed information on the adsorption process of As ions over the aforementioned nanocomposites, DFT calculations were conducted using the Perdew-Burke-Ernzerhof (PBE) functional [20-23] and double numerical plus polarization (DNP) as implemented in $DMol^3$ [24]. Grimme's PBE+D2 dispersion correction [25] method was employed in the computations to obtain

more accurate findings. All DFT calculations were done within the water solvent via the COSMO [26] method. The self-consistent field (SCF) computations were performed until the energy, force constant, and maximum displacement reached the thresholds of 1×10^{-5} Ha, 1×10^{-3} Ha/Å, and 5 10^{-5} Å, respectively. Although the surface reactivity and electronic structure characteristics of CNTs are sensitive to their chirality [27-28], a truncated (8,0) tube was employed to mimic CNTs in the current work. N-doped CNTs were created by replacing part of the C atoms in pristine CNT with N atoms. The N-CNT/RAFT nanocomposite was then constructed by allowing a RAFT molecule to attach to the exterior surface of N-doped CNTs. The dangling effects caused by our chosen truncated nanotube were eliminated by adding hydrogen atoms at the tips of the tube. The Hirshfeld method was used to calculate the atomic charges. The adsorption energy (Eads) values were computed using Equation (4) to determine the stability of the As over N-CNT/RAFT nanocomposite:

$$E_{ads} = E_{complex} - E_{composite} - E_{As\ ion} \quad (4)$$

where the $E_{complex}$, $E_{composite}$, and $E_{As\ ion}$ terms indicate the energy of relaxed As-adsorbed nanocomposite structure, free nanocomposite, and As^{3+} ion, respectively. The adsorption of As is thermodynamically possible if the E_{ads} value is negative. To assess the changes in enthalpy (ΔH) and Gibbs free energy (ΔG) caused by As ion adsorption, IR frequency calculations at the PBE/DNP level were performed.

3. Results and Discussion

3.1. Characterization

FTIR spectrum and 1HNMR (Figures 2 and 3) were studied to confirm the composite structure. The FTIR spectrum of RAFT, Figure 2, shows that the absorption bands emerged at 550, 1200, 1250, 1520-1375, 1780, 3000-2880, and 3700 cm^{-1} which are related to the stretching vibration of

CS, C = S, CO, C- (CH3) 2, C=O, CH and OH, indicating the successful synthesis of the RFAT agent. Figure 3 (a) shows the the H-NMR spectrum of the RAFT agent. According to the resonance spectrum shown at δ = 1.8 ppm, it relates to the four protons of the -CH3 group in the RAFT agent. The 1H-NMR spectra for N-CNT-OH are shown in Figure 3 (b), indicating a chemical shift at δ = 1.8, 4.35 ppm, corresponding to the -C H and Ar OH protons. For N-CNT-g-RA, the 1H-NMR spectrum of part C indicates two chemical shifts for the RAFT agent. In addition, the peaks δ = 1.0-2.0 ppm, 1.8-2.2 ppm, 4.1ppm can be related to -CH_3 in RAFT, -CH in N-CNT, and ArOH in N-CNT. All PAA-b-PAAM peaks can be observed in the 1H-NMR spectrum of the N-CNT-PAA-b-PAAm nanocomposite in Figure 3 (d). The peaks observed in the range δ = 1.2-2.5 ppm are related to the chain protons (CH) PAA and (CH_2) PAAm. For the N-CNT-RAFT agent in Figure 2, peaks at 540, 1090, 1350, 1480, 1710-1650, 2900, and 3300-3450cm^{-1} are attributed to CS, C = S, CO, CC, C = O, CH, Ar-H, and OH bonds. 1H NMR spectrum data changes the RAFT factor in N-CNT, as shown in Figure 2. In Model 1, AAm and AA monomers had a common polymer state through the RAFT surface method, which is used to prepare the N-CNT-RAFT agent. Extensive tests were performed to confirm the successful performance of the RAFT method in the N-CNT-RAFT agent. The values of peak for N-H and O-H groups in the FTIR spectrum with the final composite change the 1H NMR spectrum to a modified N-CNT composite, and the synthesis of this product can be successfully confirmed [29-31].

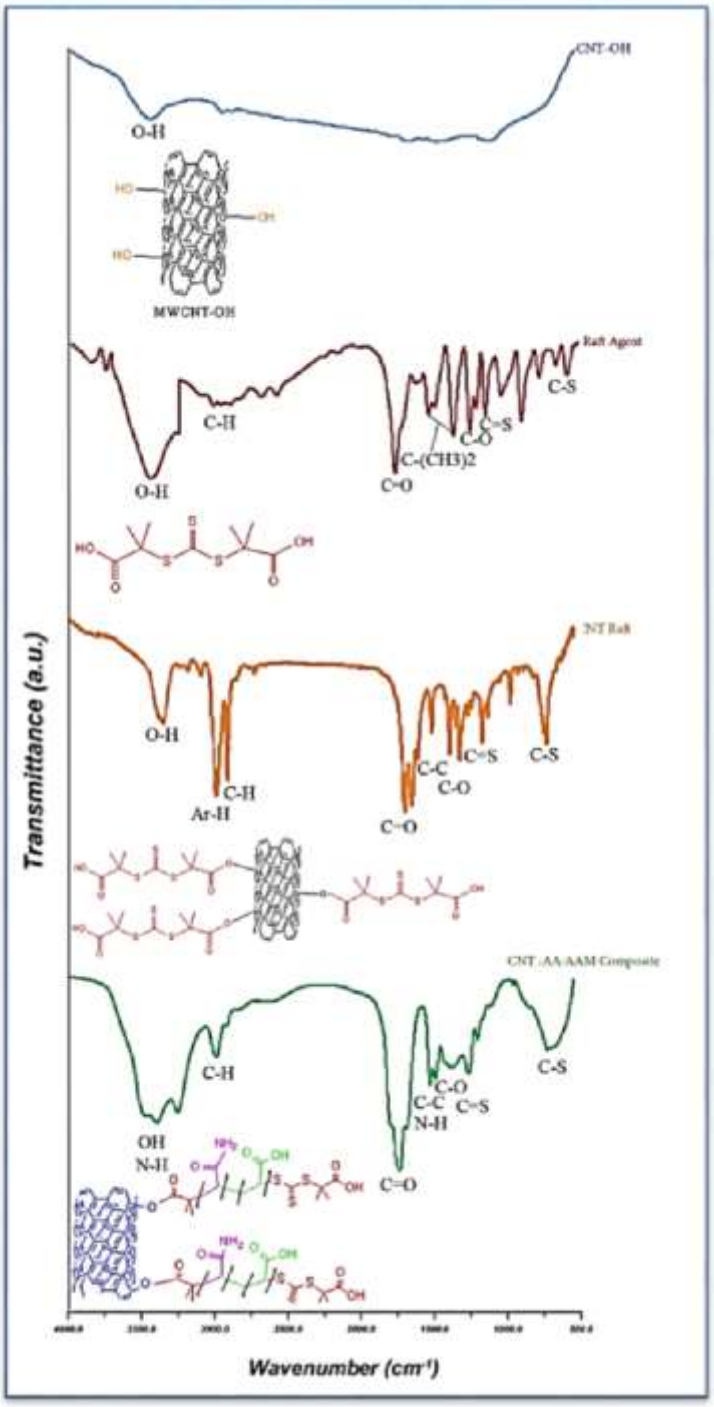

Figure 2. The FTIR spectra of synthesized compounds

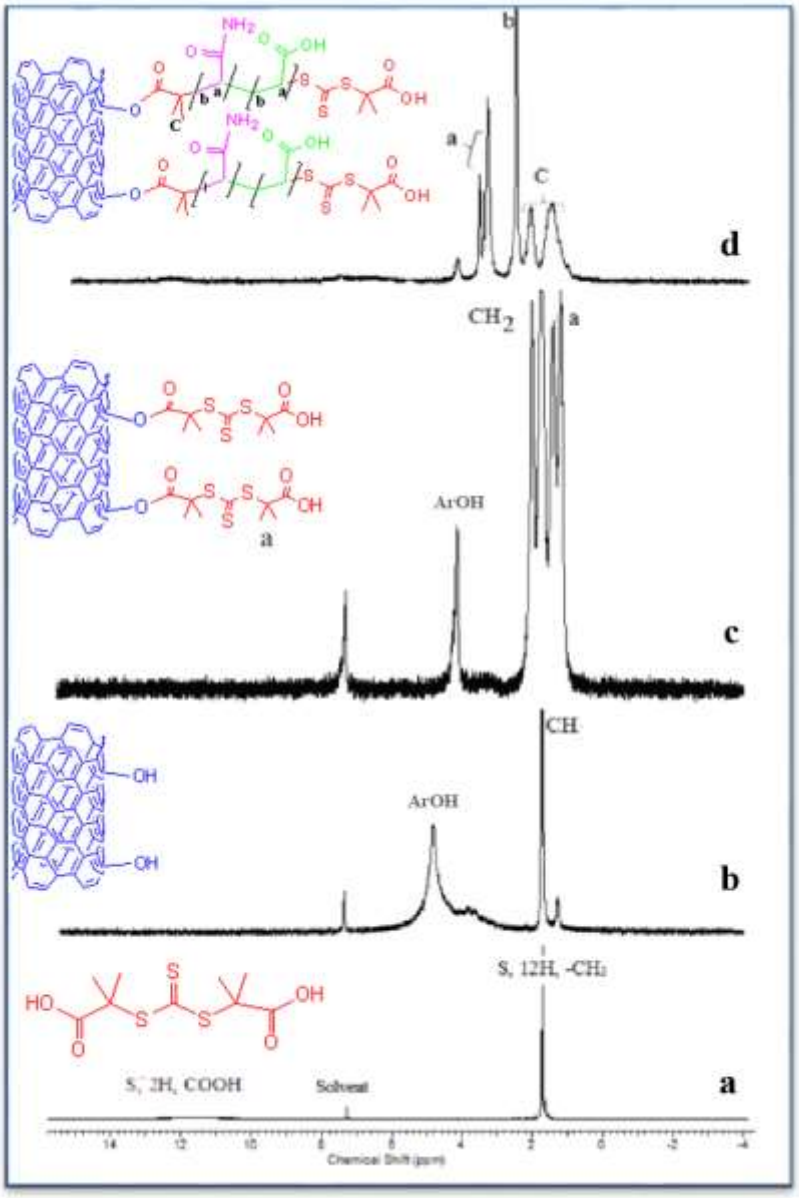

Figure 3. The 1H-NMR spectra of synthesized compounds

The TGA method was used to peruse the thermal stability and degradation pattern of the final composite. Figure 4 displays the TGA and DTG curves for N-CNT-OH, N-CNT-RAFT, and polymer/N-CNT nanocomposite. The moisture absorbed on the CNT surface caused a slight weight loss at 100 °C for N-CNT-OH. Also, the observed weight loss at 220-280 °C for N-

CNT-RAFT is due to the RAFT agent decomposition, and removal of moisture and impurities. For the polymer/N-CNT nanocomposite, two decreases in weight were detected in the DTG curve, the first peak being 210-350°C and the the other being at 360-450°C. The presence of two weight losses in the composite proved the capture of acrylic acid and acrylamide monomers on the carbon nanotubes' surface [32-33].

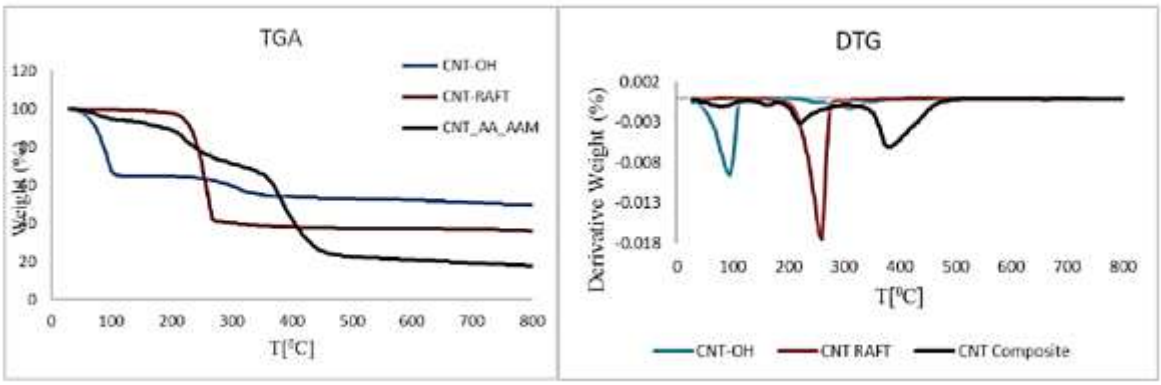

Figure 4. The TGA and DTG curves of CNT-OH, CNT-RAFT, and N-CNT-AA-AAM

The crystalline structures of N-CNT-OH nanoparticles and N-CNT/copolymers were determined using XRD patterns (Figure 5), in the diffraction range of 2θ = 10-80 °. Based on the XRD results, it can be stated that N-CNT-OH had 8 peaks at 25.4, 26.1, 42.9, 44.5, 54.1, 55.2, 62.8, and 68°, which are assigned to (002), (002), (100), (101), (110), (110), and (004) planes. In the XRD pattern of the modified N-CNT, an amorphous structure was perceived, indicating the change in the crystalline structure of the carbon nanotube [10]. These results are consistent with SEM and TEM images and indicate that N-CNT-OH is covered by polymer chains.

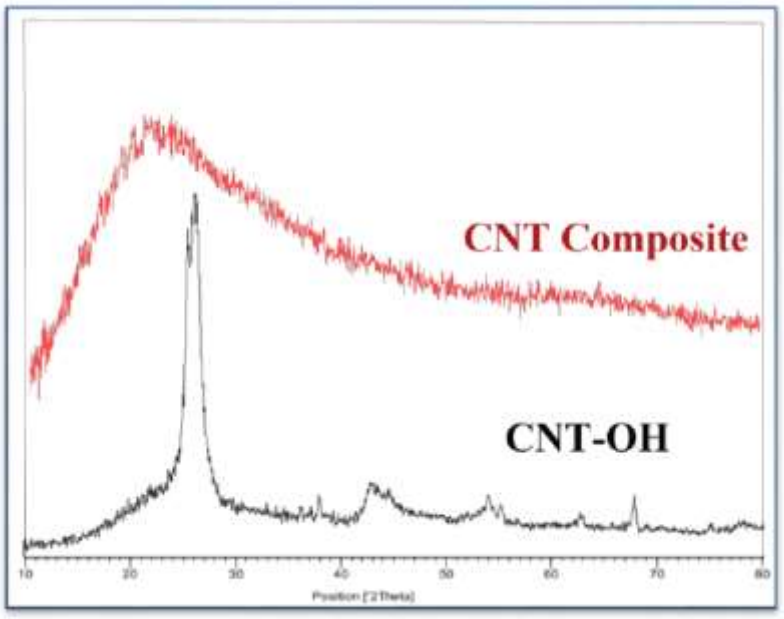

Figure 5. The X-ray diffraction pattern of the synthesized CNT-OH and the final nanocomposite

TEM and SEM images were used to analyze the morphology of the synthesized composite. Figure 6 shows the SEM (a-c) and TEM images (d-f) of the N-CNT and functionalized N-CNT. As can be seen from the TEM image (Figure 6d), the N-CNTs had an average size of 30 nm. However, the distribution of nanotubes after copolymerization was increased, as observed in the image with the single nanotubes. The TEM (Figure 4e) image demonstrates that the diameter of nanotubes increased to 100 nanometers due to the non-uniform coating of the polymer on their surface. The SEM images (4a-c) display that the carbon surface of polymer-modified nanotubes was rougher than the original nanotubes due to the accumulation of the polymer chains. In addition, SEM images also show an increase in the diameter of N-CNTs after the surface modification process.

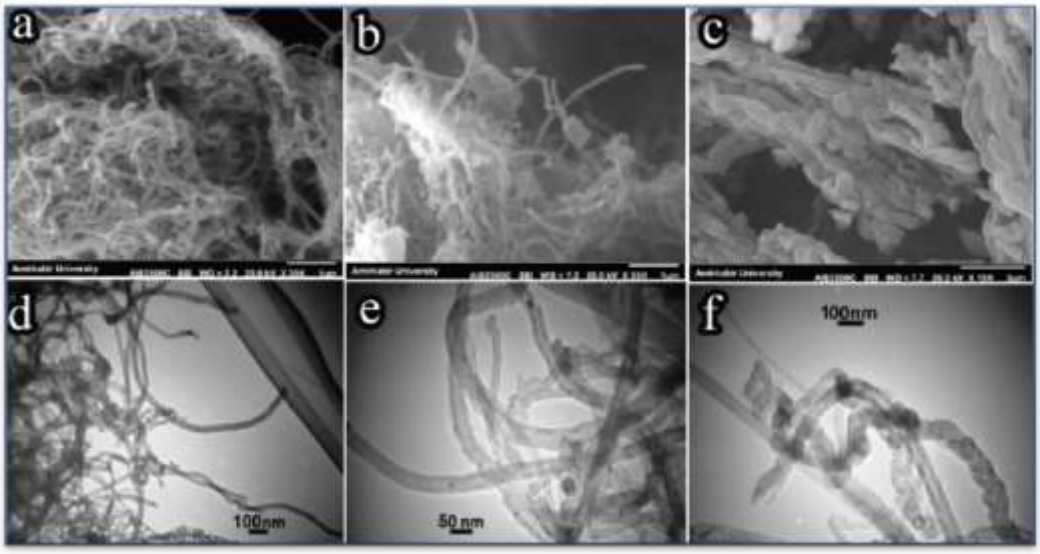

Figure 6. The SEM and TEM images of (a, d) N-CNT-RAFT agent (b, e), and polymer composite/ N-CNT (c, f)

3.2. Effect of pH on removal efficiency

The solution pH is one of the most important factors in water decontamination through adsorption processes. The pH is usually affected by the adsorbent surface charge, the ionization degree, and the change in nature of the adsorbent during the operation. The experimental parameters were designated as the initial arsenic concentration of 50 ppm, the contact time of 60 min, and the temperature of 20 °C. The pH was varied in the range of 2 and 8. At the pH above 7, Arsenic was in the form of hydroxide, which precipitated in the flask. As revealed in Figure 7, with increasing the pH, the removal efficiency increased. This can be attributed to the fact that at a low pH, due to the presence of H_3O^+, there is competition between Arsenic and H_3O^+, where, most hydrogen ions tend to interact with active surface sites and prevent the metal ions from approaching by increase of pH. However, a decrease in hydrogen protons in the solution makes competition easier and makes it easier to access active sites for Arsenic [34].

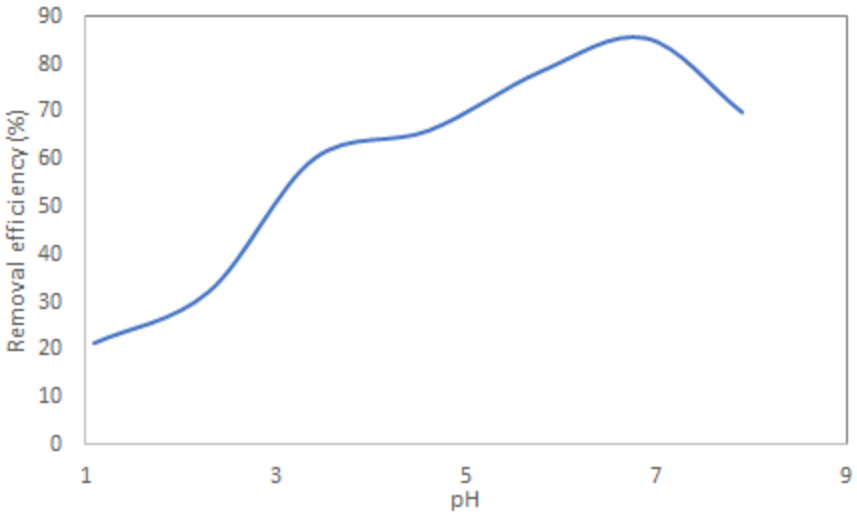

Figure 7. Effect of pH on the removal efficiency of Arsenic by nanocomposites

3.3. The effect of stirrer speed on removal efficiency

The stirrer speed was varied in the range of 100-800 rpm. The initial arsenic concentration, stirring time, and adsorbent in 100 mL of aqueous solution were 50 ppm, 60 min, and 0.1 g, respectively. The results are shown in Figure 8; when the stirrer speed increased from 100 to 400, the removal efficiency also increased. The removal efficiency was almost constant. As the stirrer speed increased to more than 500 rpm, a decrease in removal efficiency was observed. Increasing the stirrer speed increased the speed of the solution and consequently raised the speed of the ions in the aqueous solution, which reduced the interactions chance between the adsorbate/adsorbent [35].

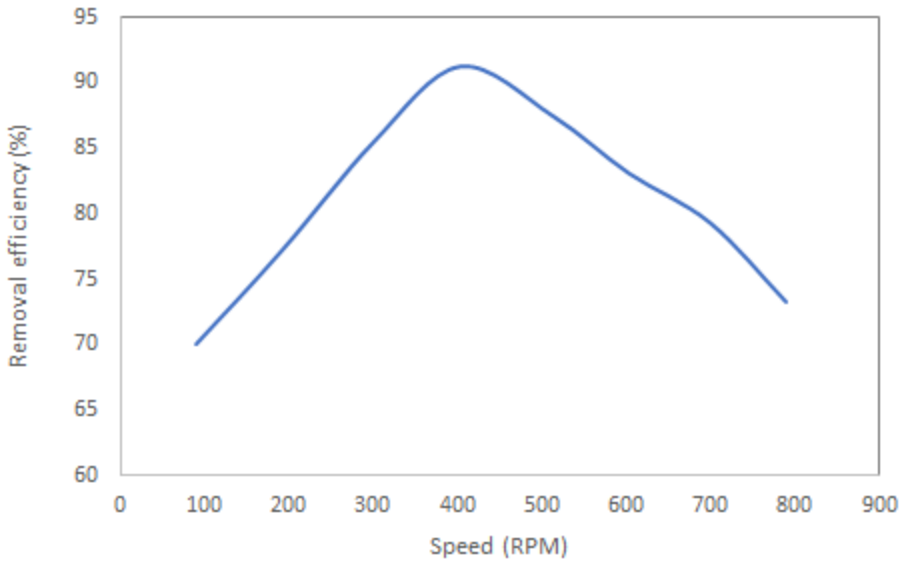

Figure 8. The effect of stirrer speed on arsenic removal efficiency by nanocomposite

3.4. Effect of contact time on removal efficiency

Figure 9 illustrates the effect of reaction time on the Arsenic adsorption. Test conditions were pH = 7, the initial concentration of 50 ppm, and the adsorbent amount was 0.1 g per 100 ml. As exposed in Figure 9, after 10 minutes, the removal efficiency reached its maximum, and after that, little change in the removal efficiency was observed. Therefore, the contact time of 10 min was selected as the optimal contact time for subsequent arsenic adsorption experiments. The maximum capacity of synthesized adsorbent was 115.2 mg/g at 10 min. It exposes that 10 min was the equilibrium time for the N-CNT nanocomposite as an adsorbent.

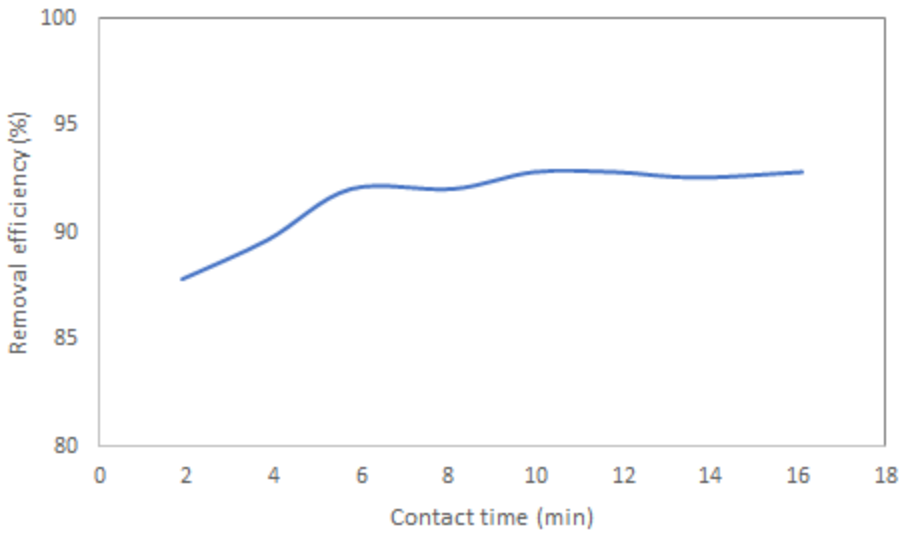

Figure 9. The effect of contact time on adsorption efficiency of the Arsenic by the adsorbents.

3.5.Effect of loaded mass on removal efficiency

To evaluate the effect of the adsorbent amount on the arsenic removal efficiency, different amounts of adsorbent (0.01- 0.16 g) in 100 mL aqueous solution, at an initial concentration of 50 ppm Arsenic, were used at the optimum pH and contact time. The results are shown in Figure 10, demonstrating that with increasing the adsorbent amount from 0.01 g to 0.1 g, the removal efficiency increased, and increasing more than 0.1 g for the adsorbent had a negligible effect on the removal efficiency. Therefore, 0.1 g per 100 ml of the aqueous solution was selected as the optimal adsorbent amount.

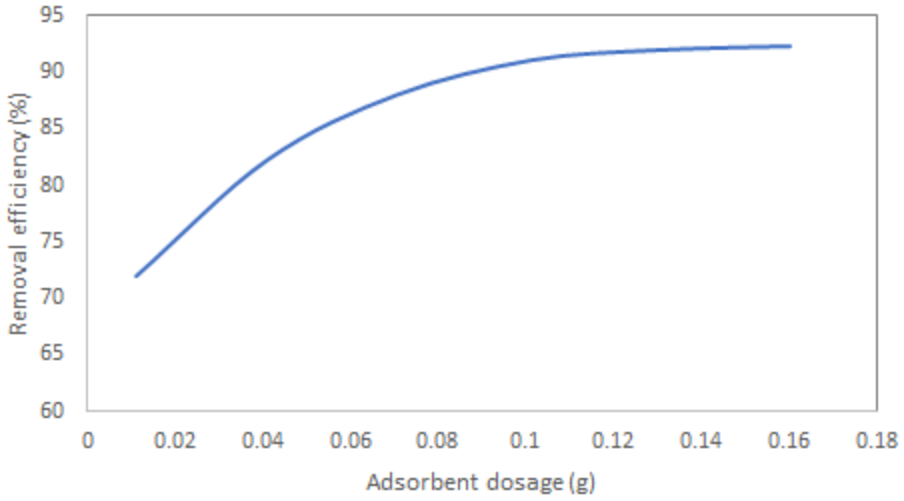

Figure 10. The effect of the adsorbent amount in aqueous solution on the removal efficiency of Arsenic by adsorbents

3.6.Effect of initial concentration on the adsorption process

Different concentrations of aqueous arsenic solutions were prepared and the adsorption process was performed under optimal conditions. The initial concentration range was selected between 20-200 ppm. The results can be seen in Figure 11, where, with increasing the concentration of Arsenic in the solution, the adsorption capacity increased, but after a concentration of 140 ppm Arsenic, the adsorption capacity became fixed, and no significant change was observed. Actually, when concentration increases, the lack of surface and active sites for adsorption at high concentrations causes more negligible adsorption. Finally, increasing the concentration increased the adsorption capacity until the surface and active sites were all occupied by the adsorbate, but when all sites were filled, the increase in the concentration no longer affected the adsorption capacity [70].

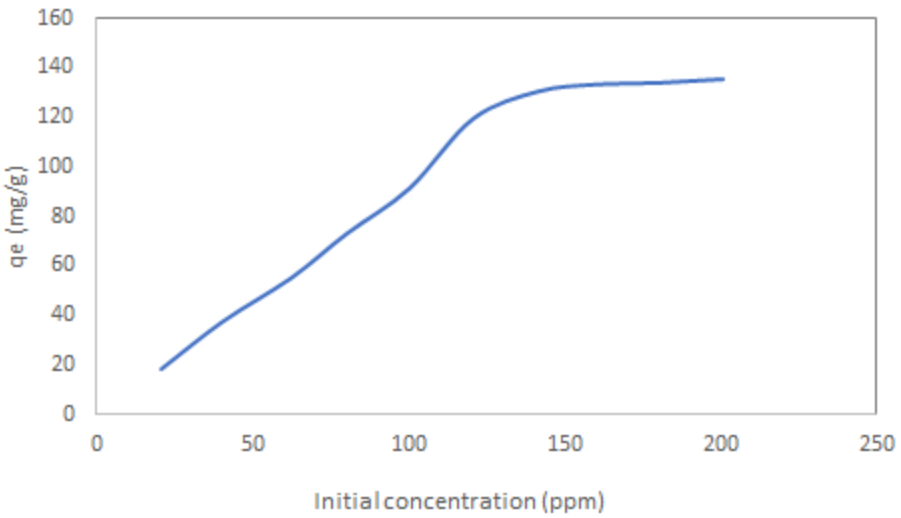

Figure 11. The effect of initial concentration on adsorption capacity of Arsenic by the adsorbent

3.7.The temperature effect

The temperature effect = on the adsorption efficiency was investigated in the temperature range of 20-50 °C. The contact time of 10 minutes, adsorbent amount of 0.1 g per 100 ml, and the initial arsenic concentration of 50 ppm were selected. The results are shown in Table 1, in which increasing the temperature improved the removal efficiency, although the temperature increment was not significant. In this case, it can be inferred that due to chemical adsorption, increasing the temperature had a positive effect on the removal efficiency.

Table 1. Effect of temperature on adsorption efficiency of Arsenic by adsorbent

Temperature (ºC)	Removal efficiency (%)
23	91.25
38	93.57
49	95.03

3.8.Adsorption kinetics

Most of the adsorption phenomena with different adsorbents are time-dependent. To understand the reaction dynamics and predict the adsorption state with time, it is essential to decipher the kinetics of these processes. Several kinetic models are used for adsorption to describe discontinuous processes, but due to the great mathematical complexity of these models, they cannot be easily used. In this regard, the reactions in which q_t changes over time can be more easily and simply used to study adsorption kinetics. The models used in this field are quasi-quadratic and Weber Morris kinetic equations. Of course, in the quadratic equations of the first and second-order, it is assumed that the difference between q_t and q_e is the main force for the absorption process, which is also proportional to the absorption amount. Both of these equations have been widely used to study experimental data derived from the adsorption of dyes, anions, and metals from aqueous solutions on various adsorbents. The Weber Morris equation is used to investigate the effect of diffusion on process kinetics. The adsorption process from an aqueous solution takes place in several stages and the general adsorption process may be controlled by one of several stages. The first step involves the adsorbate diffusion from the solution into the external adsorbent surface, and the second step is the penetration into the cavity; if second step dominates the

adsorption behavior, the process can be investigated using the Weber Morris equation. The third step comprises the diffusion into the adsorbent surface. In general, the third step states that the final equilibrium occurs based on the very low concentration of adsorbate in solution and the reduction of active sites in the adsorbent for adsorption. The Weber Morris equation is presented in the form of Equation 2:

$$q_t = K_{id}(t)^{0.5} + C \quad (1\text{-}3) \qquad (2)$$

where q_t is the absorption capacity at different times (t). The plot of the q_t versus $t^{0.5}$ is given in Figure 12. The constant value of K_{id} can be obtained by calculating the slope of this line. The Weber Morris equation constant for arsenic adsorption is K= 0.433 min^{-1} and the correlation coefficient is 0.967.

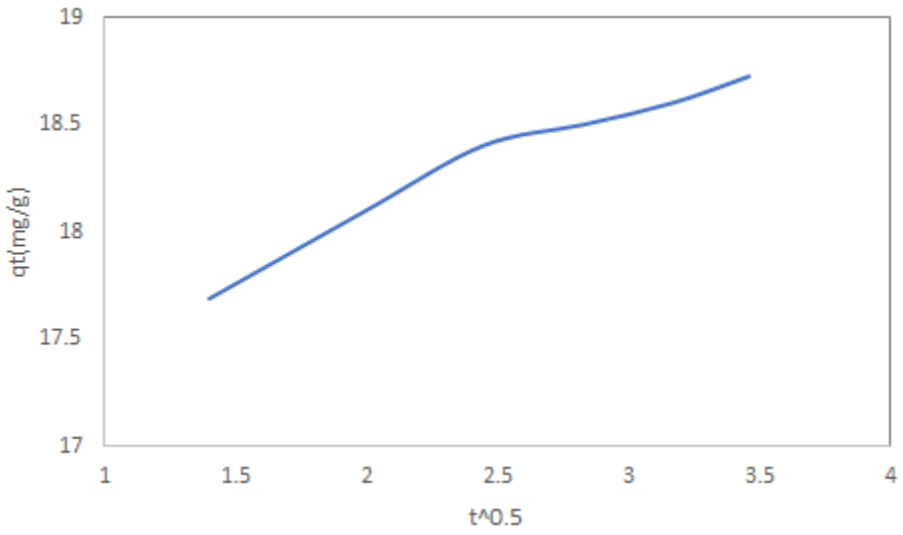

Figure 12. The Weber Morris linear equation diagram for arsenic adsorption.

The quasi-first linear Equation of Equation 2 is presented in Equation (3):

$$\log(q_e - q_t) = \log q_e - \frac{K_1 t}{2.303} \qquad (3)$$

where q_e and q_t are based on the previous definitions and K1 is a constant of this Equation. In this Equation, also by plotting the log (q_e-q_t) versus t, the constant of this Equation can be obtained (Figure 13). The constant of the quasi-quadratic Equation for arsenic adsorption is K_1= 0.26 min^{-1}, and the correlation coefficient is 0.972.

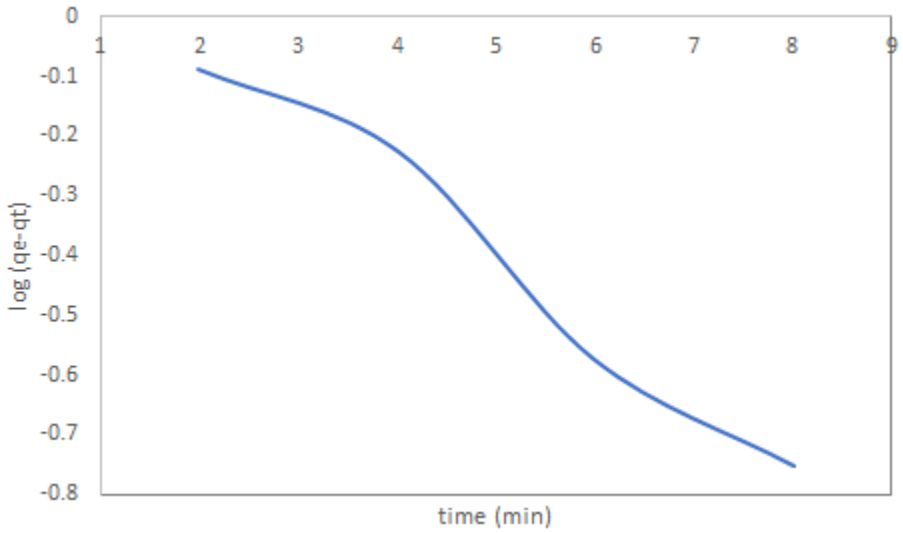

Figure 13. The scheme of a quasi-first linear equation for arsenic adsorption on the adsorbent

$$\frac{t}{q_t} = \frac{1}{k_2 q_e^2} + \frac{t}{q_e} \qquad (4)$$

By plotting the t/q_t versus t, linearization of this Equation can be done. Then, by using the slope of the line, q_e, and then by calculating the intercept and having the value of q_e, the constant of this Equation can be easily obtained (14).

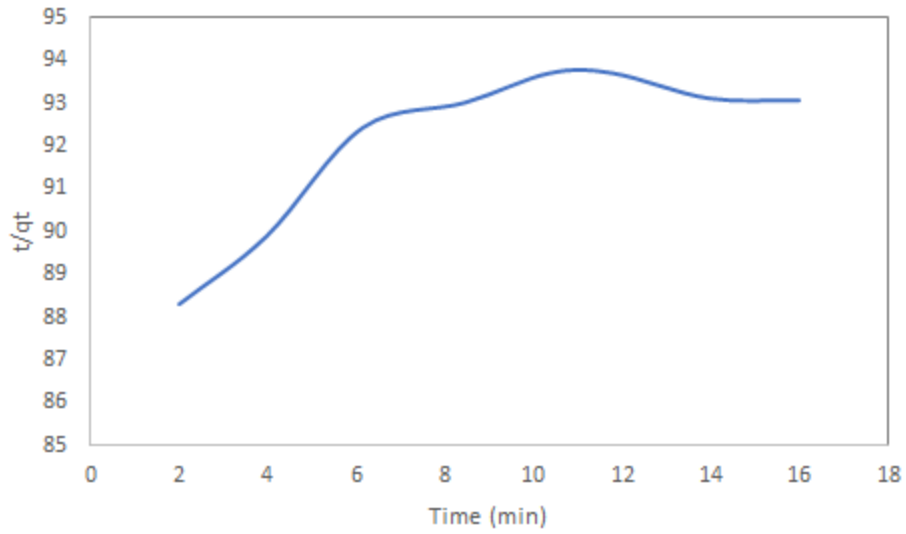

Figure 14. The scheme of a quasi-quadratic linear equation for arsenic adsorption on the adsorbent

The quasi-quadratic Equation constant and the correlation coefficient for arsenic adsorption were K2 = 0.009, 0.769 min^{-1}, respectively. By comparing the data, it can be easily seen that the results are well consistent with the quasi-quadratic Equation and the Weber Morris equation, and it can be said that the adsorption process is controlled by the quadratic Equation and the Weber Morris equation. Here, two issues should be noted: first, the rate of removal is directly related to the presence of the substance in the aqueous solution and its concentration in the aqueous solution. Secondly, in the case of penetration, it can be claimed that the process is controlled by resistance to internal penetration. The second stage is penetration based on the high concentration of adsorbent in large size. As mentioned earlier, the results show an excellent correlation with the quasi-quadratic Equation and the Weber Morris equation. The quasi-quadratic Equation is the limiting step of our process, which requires the equilibrium of the gravitational force by the division of the electron or the exchange of electrons between the absorbent and the absorbate [36].

3.9.Adsorption thermodynamics

Using the data in Tables 4-5, the thermodynamics of the adsorption processes are discussed, and the Gibbs free energy (ΔG), enthalpy (ΔH), and entropy (ΔS) were acquired based on Equations (5), (6), and (7):

$$K_c = \frac{F_e}{1 - F_e} \qquad (5)$$

$$\log K_c = \frac{-\Delta H}{2.303RT} + \frac{\Delta S}{2.303R} \qquad (6)$$

$$\Delta G = -RT \ln K_c \qquad (7)$$

In Equation (5), Arsenic is a component of a water-soluble substance that absorbs the adsorbates. The thermodynamics of the adsorbate removal process are given in Table 2. As can be seen, the ΔG of these processes was negative, which indicates that these processes were spontaneous. A positive ΔH also indicates that these two processes were calorific. A positive ΔS indicates that the interface between the solid and liquid phases increased randomly as ions were fixed on the adsorbent surface.

Table 2. Thermodynamic parameters of arsenic adsorption on the adsorbent

ΔH (kj/mol)	ΔS (kj/mol.K)	T °C	ΔG (kj/mol)
		23	-5.767
21.67	0.09	38	-6.923
		49	-8.182

3.10. Adsorption isotherms

The basis of the adsorption isotherm is the assumption that all adsorption sites are the same and independent of other sites, whether those sites are available or covered. Isotherms show the relationship between the adsorbate concentration in solution and the adsorbate amount at a constant temperature.

3.10.1. Langmuir isotherm

Langmuir's theory describes the monolayer coverage of the adsorbates on a homogeneous adsorbent surface. This isotherm is based on the assumption that the adsorption process occurs only once for each location. The Langmuir equation is in the form of Equation (8):

$$q_e = \frac{q_0 K_L C_e}{(1+K_L C_e)} \qquad (8)$$

Where q_e is the equilibrium adsorption capacity, Ce is the equilibrium concentration, and q_o is the maximum amount of monolayer adsorption, q_o can also be called the theoretical absorption capacity.

To find the equation constants, K_c and q_o, this Equation must be linearized. The linearization form of this isotherm is given in Equation (9):

$$\frac{C_e}{q_e} = \frac{1}{q_0 .K_L} + \frac{1}{q_0} C_e \qquad (9)$$

By plotting the C_e/q_e versus C_e, a line is obtained, the slope and intercept of which indicate the q_o and K_L, respectively. The adsorption results of Arsenic are given in Figure 15. As can be seen, the slope of the line for Arsenic was negative, and the correlation coefficient was very low, which practically shows that this Equation is not suitable to explain this adsorption process [36-37].

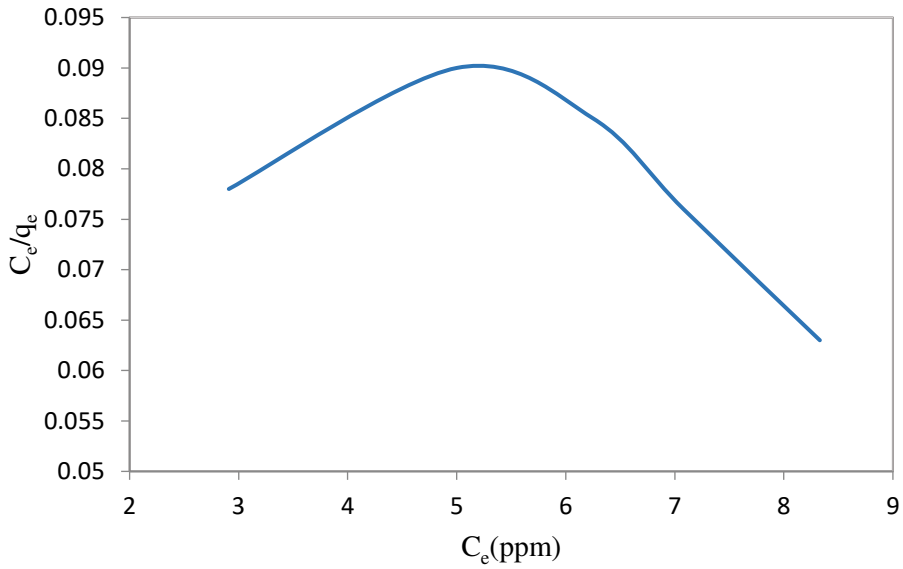

Figure 15. The Langmuir linear equation for arsenic adsorption on the adsorbent

3.10.2. Freundlich isotherm

The Freundlich equation, in contrast to the Langmuir, is based on a non-homogeneous or heterogeneous surface. The Langmuir equation assumes that the enthalpy of adsorption is independent of the amount of adsorption, but in the Freundlich isotherm, it is assumed that the enthalpy of adsorption decreases logarithmically with increasing the number of occupied spaces. The Freundlich isotherm equation is given in Equation (10):

$$q_e = K_F\,(C_e)^{1/n} \qquad (10)$$

The K_F and 1/n are the Freundlich constant and the adsorption intensity, respectively. To obtain this constant, we must first linearize this Equation, which is presented in Equation (11):

$$\log(q_e) = \log(K_F) + \frac{1}{n}\log(C_e) \qquad (11)$$

By calculating the line slope and intersection, n and K_F can be obtained. The results for the arsenic adsorption on the adsorbent are presented in Table 3. The constants of the Freundlich equation, K_F and n, determine all the factors affecting the adsorption process, such as adsorption capacity and adsorption intensity. Figure 16 shows the linear model of this Equation for the arsenic adsorption on the adsorbents

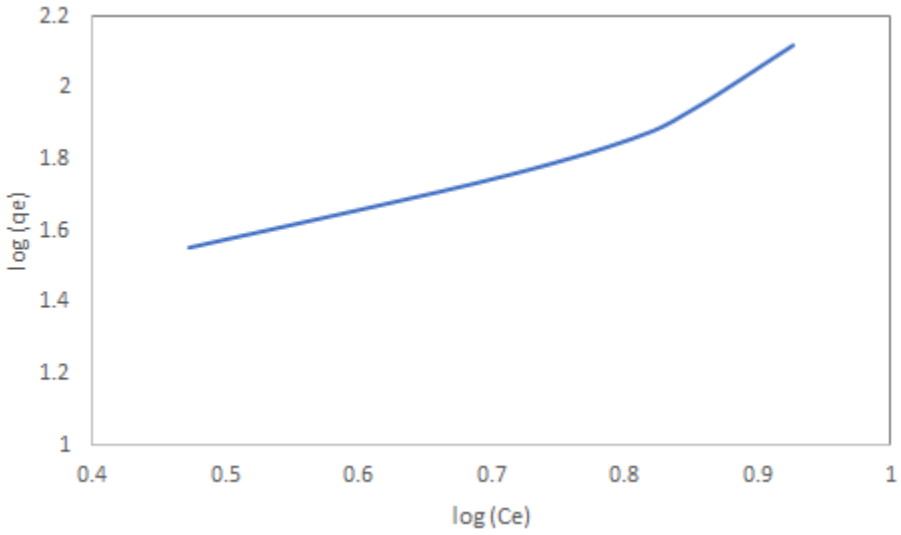

Figure 16. The Freundlich linear equation describing the arsenic adsorption on the adsorbents

3.11. Dublin Radushkevich Model (D-R)

The Dublin Radushkevich model is used for data analysis. The linear shape of this model is presented in Equation (12):

$$\ln(q_e) = \ln(q_m) - \beta\varepsilon^2 \qquad (12)$$

In this Equation, q_e is the equilibrium absorption capacity, q_m is the maximum absorption capacity of the theory, and β is the constant of the Equation [38].

$$\varepsilon = RT \ln\left[1 + \left(\frac{1}{C_e}\right)\right] \qquad (13)$$

where R is the global constant of gases and T is the temperature in Kelvin and Ce is the equilibrium concentration. By plotting $\ln q_e$ in terms of 2ε, the values of q_m and β can be calculated using the slope and intersection (Fig. 17). These equations for arsenic adsorption on the adsorbent are given in Table 3, respectively.

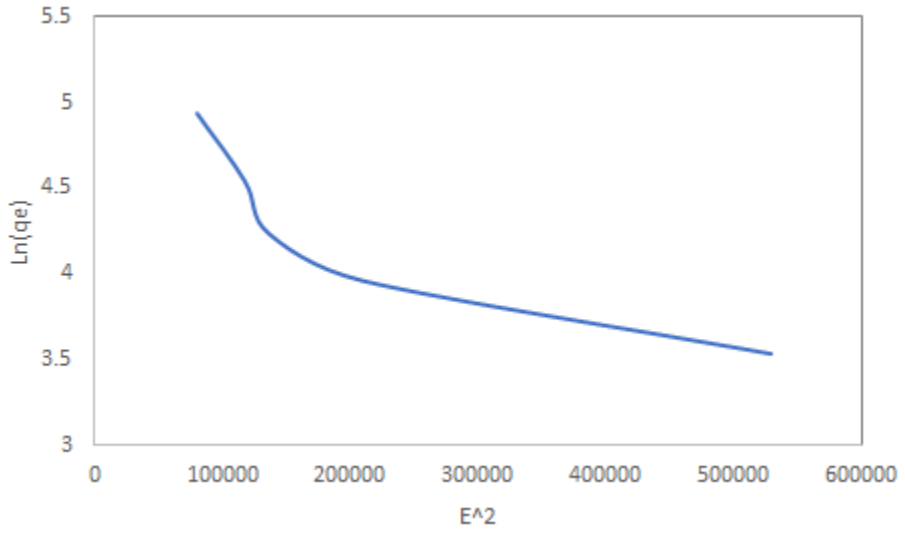

Figure 17. Drawing the D-R linear Equation for arsenic adsorption on the adsorbent

Table 3. Equations and constants of adsorption isotherms for arsenic adsorption.

	Langmuir equation	r^2
	y = 0.0027x + 0.0947	0.3079
	Freundlich parameter	
K_F	N	r^2
9.78	0.87	0.9429
	D-R parameter	
q_m (mg/g)	B	r^2
115	$2*10^{-6}$	0.7828

As can be seen, the results show the best agreement with the Freundlich isotherm. However, it should be noted that the Freundlich equation provides information about the inhomogeneous surface and the exponential distribution of active sites and their energy, but this Equation cannot predict the saturation of the adsorbent surface. Regarding the Dublin Radushkevich equation, it should be noted that the correlation coefficient of this Equation is considerable, and by using this Equation, which relates the heterogeneity of energy to the surface, surface saturation can be predicted.

Table 4. The adsorption energy (E_{ads}), changes of Gibbs free energy (ΔG), and enthalpy (ΔH) due to the As^{3+} ion adsorption on different substrates.

substrate	E_{ads} (kJ/mol)	ΔG (kJ/mol)	ΔH (kJ/mol)
N-CNT	-121.0	-40.2	-52.8
N-CNT/RAFT(**A**)	-135.1	-42.5	-56.7
N-CNT/RAFT(**B**)	-128.5	-41.4	-54.9
N-CNT/RAFT(**C**)	-140.7	-43.9	-58.0

3.12 DFT results

DFT calculations can provide useful information regarding the As^{3+} ion adsorption characteristics of N-CNT/RAFT nanocomposite. To achieve this goal, dispersion-corrected DFT calculations were performed on some molecular models of the aforementioned systems. As previously mentioned, N-CNT was generated by substituting some of the carbon atoms in pristine (8,0) CNT with nitrogen. In accordance with other similar DFT investigations [39-40], the average optimized C–N and C–C bond lengths in the N-CNT are 1.42 and 1.39 Å, respectively. To examine the effect of RAFT addition on As^{3+} ion adsorption, we first looked at As^{3+} ion adsorption on N-CNT. Figure 18 (a) illustrates the optimized structure, while Table 4 summarizes the adsorption energy (E_{ads}), changes in Gibbs free energy (ΔG), and enthalpy (ΔH) due to As^{3+} ion adsorption. Our findings show that an As^{3+} ion preferentially adsorbs on the carbon atoms at the tips of the N-CNTs. This is most likely owing to the higher negative charge localization on these atoms compared to others. Meanwhile, the adsorption energy of -121 kJ/mol was found for the As^{3+} ion, suggesting that the As^{3+} ion has a quite strong interaction with the N-CNT. The Hirshfeld charge on the As^{3+} ion decreased to +0.27 |e| after adsorption, suggesting that As^{3+} adsorption is followed

by a charge transfer from the N-CNT into As. The results also show that adsorption of the As^{3+} ion is thermodynamically feasible due to the associated negative ΔG and ΔH values.

We attached a RAFT moiety to different parts of the N-CNT to determine whether it might increase its surface reactivity towards the As^{3+} ion. According to our calculations, there are two most stable positions for attaching a RAFT species to the surface of the N-CNT. The first one is on the carbon atom, which is placed between two nitrogen atoms. In Figure 18(b), this configuration is labeled **A**. The RAFT moiety is bonded to the carbon atom via its O atom of carboxylic group in this configuration. The newly formed C–O bond between the RAFT and N-CNT was 1.46 Å and the calculated adsorption energy was -140.5 kJ/mol. On the other hand, it is shown that the RAFT can also be bonded to the carbon atom at the tip of N-CNT (configuration **B**). The adsorption energy for this configuration was -158.9 kJ/mol, which is more than the corresponding value of configuration **A**. That is, the carbon atoms at the tips are more active than those in the center of N-CNT. When an As^{3+} ion is added to the N-CNT/RAFT nanocomposites, it prefers to be placed between the O atoms of the carboxylic and amide groups. The E_{ads} values of the As^{3+} ion on the N-CNT/RAFT are larger than on the bare N-CNT, indicating that the presence of the RAFT moiety modifies the adsorption characteristics of N-CNT. Furthermore, higher negative ΔG and ΔH values owing to As^{3+} ion adsorption clearly suggest that the N-CNT/RAFT nanocomposite had a better performance for removing As^{3+} ions from aqueous environments.

Previous DFT investigations [41-42] have indicated that the surface reactivity of N-CNTs is enhanced in the presence of monovacancy defects produced during synthesis. To investigate the effect of such vacancy defects on the adsorption of As^{3+} ion, we introduced a monovacancy defect on the N-CNT and then allowed a RAFT molecule to bind to it (configuration C). The inclusion of a defect affected the charge density over the RAFT moiety, altering the As^{3+} adsorption energy.

As shown in Table 4, the presence of a monovacancy defect further increased the values of E^{ads}, ΔG, and ΔH, suggesting that monovacancy defects on the surface of N-CNTs may also promote the removal of As^{3+} ions.

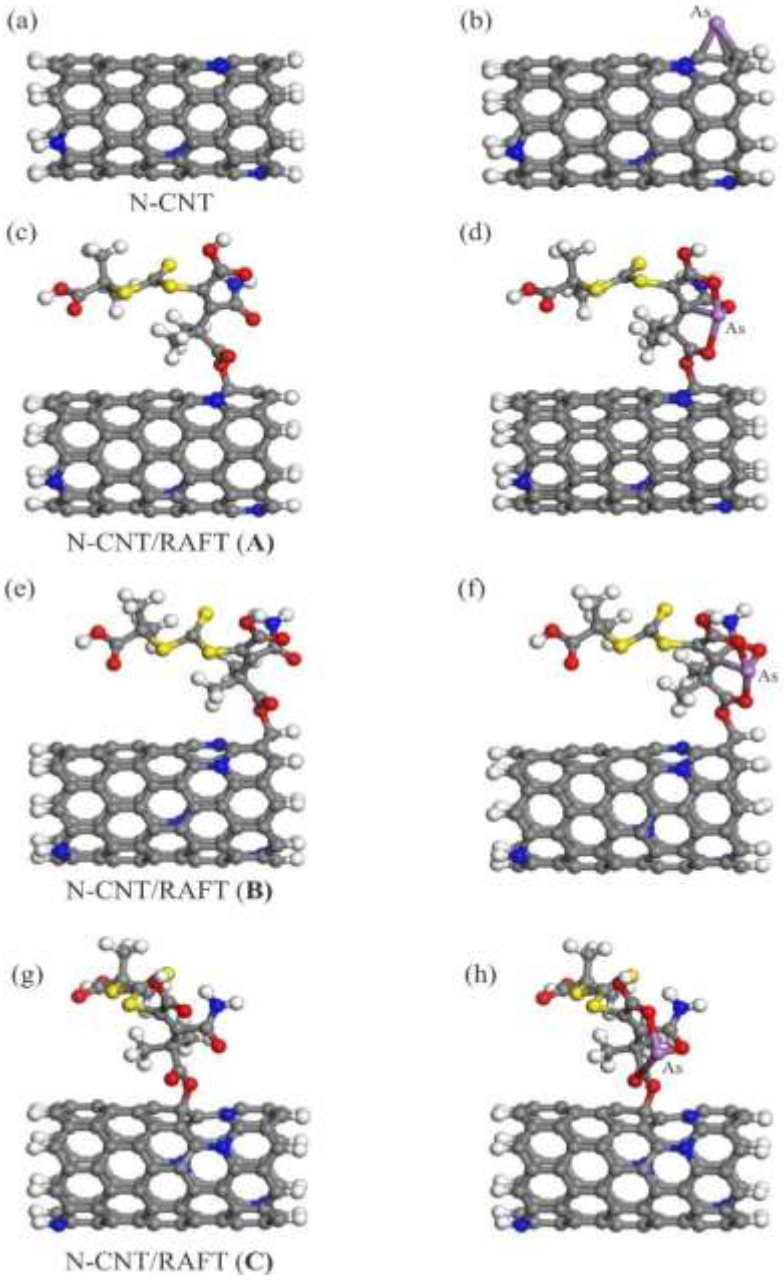

Figure 18. The optimized structure of (a) N-CNT, (b) As3+ adsorbed N-CNT, (c) N-CNT/RAFT (A), (d) As3+ adsorbed N-CNT/RAFT (A), (e) N-CNT/RAFT (B), (f) As3+ adsorbed N-CNT/RAFT (B), (g) N-CNT/RAFT (C) and (h) As3+ adsorbed N-CNT/RAFT (C). The color code of atoms: gray (C), red (O), yellow (S), violet (As), blue (N) and white (H).

4. Conclusion

The investigation of heavy metal adsorption was carried out for environmental protection. For this aim, the N-CNT/polymer nanocomposite was synthesized using the RAFT method and the N-CNT-RAFT precipitation agent. The results showed that N-CNT/polymer nanocomposite had significant potential for adsorbing Arsenic from the water. In addition, simulation of adsorption mechanism by DFT software was done to validate the experimental data. Moreover, the effective parameters were assessed in the arsenic adsorption process, including pH, contact time, initial metal concentration, and adsorption temperature. By increasing the pH, the removal efficiency increased, owing to the competition between Arsenic and H_3O^+, the active sites of the surface interacted by hydrogen ions and avoid the metal ions from approaching by increasing the pH. The maximum capacity of the nanocomposite adsorbent was 115.2 mg/g at 10 min. Numerous kinetic models were used for arsenic adsorption in batch processes. The adsorption kinetics revealed that the Arsenic adsorption followed the Pseudo-First order and Weber Morris equation. The results displayed the best consistency with the Freundlich isotherm in the isothermic studies. It is notable that the Freundlich equation affords information about the inhomogeneous surface and the exponential distribution of active sites and their energy. The results showed that increasing the temperature in this process can also increase the removal efficiency, indicating the occurrence of the chemical adsorption. From the DFT calculations, it was found that, introducing the RAFT agent to the N-CNT surface improves the interaction between N-CNT and Arsenic ions. In addition, a monovacancy defect can further ameliorate the adsorption performance, indicating the effective role of monovacancy the surface of N-CNTs in promoting the removal of As^{3+} ions.

References

[1] T. Fujibayashi, M. Okubo, Preparation and thermodynamic stability of micron-sized, monodisperse composite polymer particles of disc-like shapes by seeded dispersion polymerization, Langmuir, 23 (2007) 7958-7962.

[2] X. Jiang, A. Yu, W. Yang, Y. Ding, C. Xu, S. Lam, Synthesis and growth of hematite nanodiscs through a facile hydrothermal approach, Journal of nanoparticle research, 12 (2010) 877-893.

[3] D.J. Kinning, K.I. Winey, E.L. Thomas, Structural transitions from spherical to nonspherical micelles in blends of poly (styrene-butadiene) diblock copolymer and polystyrene homopolymers, Macromolecules, 21 (1988) 3502-3506.

[4] S. Koizumi, H. Hasegawa, T. Hashimoto, Ordered structures of block copolymer/homopolymer mixtures. 5. Interplay of macro-and microphase transitions, Macromolecules, 27 (1994) 6532-6540.

[5] S. Liu, J. Zhou, L. Zhang, J. Guan, J. Wang, Synthesis and alignment of iron oxide nanoparticles in a regenerated cellulose film, Macromolecular rapid communications, 27 (2006) 2084-2089.

[6] M. Okubo, T. Fujibayashi, A. Terada, Synthesis of micron-sized, monodisperse polymer particles of disc-like and polyhedral shapes by seeded dispersion polymerization, Colloid and Polymer Science, 283 (2005) 793-798.

[7] D.H., Nguyen, P., Vana, Silica-immobilized cumyl dithiobenzoate as mediating agent in reversible addition fragmentation chain transfer (RAFT) polymerization. Polym. Adv. Technol. 17 (2016) 625–633.

[8] Y. Peng, Z. Liu, Z. Yang, Polymer-Controlled Growth of CuO Nanodiscs in the Mild Aqueous Solution, Chinese Journal of Chemistry, 27 (2009) 1086-1092.

[9] R. Subba, V. Ch, K.-I. Park, S.-i. Mho, I.-H. Yeo, S.-M. Park, Simple Preparation of V 2 O 5 Nanostructures and Their Characterization, Bulletin of the Korean Chemical Society, 29 (2008) 2061-2064.

[10] M. Wang, S.H. Hahn, J.S. Kim, J.S. Chung, E.J. Kim, K.-K. Koo, Solvent-controlled crystallization of zinc oxide nano (micro) disks, Journal of Crystal Growth, 310 (2008) 1213-1219.

[11] J.J. Zhang, G. Jin, Y. Ma, Phase separations in a copolymer–copolymer mixture, Journal of Physics: Condensed Matter, 18 (2005) 837.

[12] Y. Zhu, H. Yu, J. Zhu, G. Zhao, W. Jiang, X. Yang, Morphological transition of dry vesicles into onion-like multilamellar micelles induced through heating at high temperature, Chemical Physics Letters, 460 (2008) 257-260.

[13] V.K., Gupta, I., Tyagi, S., Agarwal, O., Moradi, H., Sadegh, R.,Shahryari-Ghoshekandi, A., Garshasbi, Study on the removal of heavy metal ions from industry waste by carbon nanotubes: effect of the surface modification-a review. Crit. Rev. Environ. Sci. Technol. 15 (2015) 1–26.

[14] E.M., Elsehly, N.G., Chechenin, A.V., Makunin, H.A., Motaweh, E.G., Leksina, Functionalized carbon nanotubes based filters for chromium removal from aqueous solutions. Water Sci. Technol. 75 (2017) 1564–1571.

[15] S.T. Ha, O.O. Park, S.H. Im, Size control of highly monodisperse polystyrene particles by modified dispersion polymerization, Macromolecular research, 18 (2010) 935-943.

[16] M.N., Mujawar, J.N., Sahu, E.C., Abdullah, J., Natesan, Removal of heavy metals from wastewater using carbon nanotubes. Sep. Purif. Rev. 43 (2014) 311–338.

[17] Ghasemy, E., Motejadded, H. B., Hamzehlouyan, T., & Yousefian, Z. (2018). N-doped CNT nanocatalyst prepared from camphor and urea for gas phase desulfurization: experimental and DFT study. Journal of the Taiwan Institute of Chemical Engineers, 85, 121-131.

[18] X. Zhang, S. Shen, L. Fan, Uniform polystyrene particles by dispersion polymerization in different dispersion medium, Polymer Bulletin, 61 (2008) 19-26.

[19] L.A. Fielding, J.A. Lane, M.J. Derry, O.O. Mykhaylyk, S.P. Armes, Thermo-responsive diblock copolymer worm gels in non-polar solvents, Journal of the American Chemical Society, 136 (2014) 5790-5798.

[20] A. Sarkar, J. Bhagat, and S. Sarker, “Evaluation of impairment of DNA in marine gastropod, Morula granulata as a biomarker of marine pollution,” Eco. and Enviro. Saf., 106 (2014) 253–261.

[21] S. Pashaei, S. Hosseinzadeh, A.A. Syed, Studies on coconut shell powder and crysnanoclay incorporated acrylonitrile-butadiene rubber/styrene butadiene rubber (NBR/SBR) green nanocomposites. Polym. Compos. 37 (2015) 1–9.

[22] S., Saber-Samandari, S., Saber-Samandari, Cellulose-graft polyacrylamide/hydroxyapatite composite hydrogel with possible application in removal of Cu (II) ions. React. Funct. Polym. 73 (2013) 1523–1530.

[23] J.P. Perdew, K. Burke, M. Ernzerhof, Generalized gradient approximation made simple, Phys. Rev. Lett., 77 (1996) 3865.

[24] A.M., Stanescu, L., Stoica, C., Constantin, L., Lacatusu, O., Oprea, F., Miculescu,. Physicochemical characterization and use of heat pretreated commercial instant dry Baker's Yeast as a potential biosorbent for Cu(II) removal. Clean Soil Air Water 42 (2014) 1632–1641.

[25] S. Grimme, Accurate description of van der Waals complexes by density functional theory including empirical corrections, J. Comput. Chem., 25 (2004) 1463-1473.

[26] J., Guo, W., Yang, C., Wang, Magnetic colloidal supraparticles: design, fabrication and biomedical applications. Adv. Mater. 25 (2013) 5196–5214.

[27] A.N. Chermahini, A. Teimouri, H. Farrokhpour, A DFT-D study on the interaction between lactic acid and single-wall carbon nanotubes. RSC advances, 5 (2015) 97724-97733.

[28] G. R. Ahmed Jamal, M. Rezanur Islam, M. Adnan Rahman, J. Ferdous Meem, and R. Akter Sathie. "Chirality dependence of gas adsorption property of single wall carbon nanotubes." In Materials Science Forum, vol. 889, pp. 248-252. Trans Tech Publications Ltd, 2017.

[29] G.P.Rao, C.Lu, F. Su,sorption of divalent metal ions from aqueous solution by carbon nonotubes: A review, Sepration and Purification Technology 58(1) ,2007, 224-231.

[30] D. Tasis, N. Tagmatarchis, A. Bianco, M. Prato, Chemistry of Carbon Nanotubes, Chem. Rev. 106(3) 2006 1105-1136.

[31] V.A. Karachvtsev, A. Yu. Glamazda, U. Dettlaff-Weglikowska, V.S. Leontiev, A.V.Peschanskii, Plokhotnichenko, S.G Stepanian and S. Roth, Spectroscopy of Emerging Materials, Springer Netherlands, 165 (2006) 139.

[32] M. F. Islam, E.Rojas, D. M. Bergey, A. T. Johnson, A. G. Yodh, High weight fraction surfactant solubilization of single-wall carbon nanotubes in water, Nano Lett 3 (2003) 269.

[33] N. G. Sahooa, S. RAnab, J. W. Chob, L. Li, S. H. Chana, Polymer nanocomposites based on functionalized carbon nanotubes, progress in Polymer science 35 (2010) 837.

[34] F., Zhao, X., Qin, S., Feng, Preparation of microgel/sodium alginate composite granular hydrogels and their Cu2+ adsorption properties. RSC Adv. 6 (2016) 100511–100518.

[35] R.X.,Wang, J.J., Men, B.J., Gao, Synthesis and characterization of magnetic metalorganic framework for the adsorptive removal of Rhodamine B from aqueous solution. Clean Soil Air Water 40 (2012) 278–284.

[36] A. Kongsuwan, P. Patnukao, P. Pavasant, Binary component sorption of Cu (II) and Pb(II) with activated carbon from eucalyptus camaldulensis Dehn bark, J. Ind. Eng. Chem. 15 (2009) 465–470.

[37] M.O. Abd El-Magied, S. Dhmees Abdelghaffar, M. Abd Allah, E. Abd, E.M. Eldesouky, Uranium extraction by sulfonated mesoporous silica derived from blast furnace slag, J. Nucl.. Mat. 509 (2018) 295–304.

[38] E.A. Elshehy, M.A. Shenashen, M.O. Abd El-Magied, A.M. El-Nahas, D.A. Tolan, K. Halada, A.A. Atia, S.A. El-Safty, Selective recovery of silver (I) ions from e-waste using

cubically multi-thiolated cage mesoporous monoliths, Eur. J. Inorg. Chem. 2017 (2017) 4823–4833.

[39] M.D. Esrafili, Nitrogen-doped (6, 0) carbon nanotubes: a comparative DFT study based on surface reactivity descriptors. Comput. Theor. Chem. 1015 (2013) 1-7.

[40] C. Zhao, X. Zhou, S. Xie, H. Wei, J. Chen, X. Chen, C. Chen, DFT study of electronic structure and properties of N, Si and Pd-doped carbon nanotubes. Ceramics International, 44 (2018) 21027-21033.

[41] Q. Zhou, C. Wang, Z. Fu, H. Zhang, Y. Tang, Adsorption of formaldehyde molecule on Al-doped vacancy-defected single-walled carbon nanotubes: a theoretical study. Comput. Mater. Sci., 82 (2014) 337-344.

[42] A. I. Vasylenko, M. V. Tokarchuk, S. Jurga, Effect of a vacancy in single-walled carbon nanotubes on He and NO adsorption. J. Phys. Chem. C, 119 (2015) 5113-5116.